Shear stress- and line length-dependent screw dislocation cross-slip in FCC Ni

Shuozhi Xu[a,*], Liming Xiong[b], Youping Chen[c], David L. McDowell[a,d]

[a] *GWW School of Mechanical Engineering, Georgia Institute of Technology, Atlanta, GA 30332-0405, USA*
[b] *Department of Aerospace Engineering, Iowa State University, Ames, IA 50011, USA*
[c] *Department of Mechanical and Aerospace Engineering, University of Florida, Gainesville, FL 32611-6250, USA*
[d] *School of Materials Science and Engineering, Georgia Institute of Technology, Atlanta, GA 30332-0245, USA*

Abstract

Screw dislocation cross-slip is important in dynamic recovery of deformed metals. A mobile screw dislocation segment can cross slip to annihilate an immobile screw dislocation segment with opposite Burgers vector, leaving excess dislocations of one kind in a crystal. Previous studies have found that the cross-slip process depends on both the local stress state and dislocation line length, yet a quantitative study of the combined effects of these two factors has not been conducted. In this work, we employ both dynamic concurrent atomistic-continuum (CAC) [L. Xiong, G. Tucker, D.L. McDowell, Y. Chen, J. Mech. Phys. Solids 59 (2011) 160–177] and molecular dynamics simulations to explore the shear stress- and line length-dependent screw dislocation cross-slip in face-centered cubic Ni. It is demonstrated that the CAC approach can accurately describe the 3-D cross-slip process at a significantly

*Corresponding author
Email address: shuozhixu@gatech.edu (Shuozhi Xu)

reduced computational cost, as a complement to other numerical methods. In particular, we show that the Fleischer (FL) [R.L. Fleischer, Acta Metall. 7 (1959) 134–135] type cross-slip, in which a stair-rod dislocation is involved, can be simulated in the coarse-grained domain. Our simulations show that as the applied shear stress increases, the cross-slip mechanism changes from the Friedel-Escaig (FE) [B. Escaig, J. Phys. 29 (1968) 225–239] type to the FL type. In addition, the critical shear stress for both cross-slip mechanisms depends on the dislocation line length. Moreover, the cross-slip of a screw dislocation with a length of 6.47 nm analyzed using periodic boundary conditions occurs via only the FL mechanism, whereas a longer dislocation with length of 12.94 nm can cross-slip via either the FE or FL process in Ni subject to different shear stresses.
Keywords: Multiscale simulation, atomistic simulation, cross-slip, FCC metal, plastic deformation

1. Introduction

Cross-slip of screw dislocations is important for dynamic recovery of metals because it helps dislocations escape from obstacles and in annihilating each other at the end of stage II work hardening [1]. Without cross-slip, the dislocation density and work hardening rate would not be reduced sufficiently, resulting in a less ductile material that breaks at a smaller strain. Cross-slip is also involved in the process of dislocation bypass of preciptates [2] and voids [3], affecting the obstacle strengthening. Among many possible cross-slip mechanisms [4], including the Washburn model, the Schoeck-Seeger model, the Duesbery model, and the Püschl model, the Friedel-Escaig (FE)

[5] and Fleischer (FL) mechanisms [6] are usually considered the most prominent [7]. In the FE mechanism, the leading and trailing partial dislocations in a short segment of a screw dislocation are recombined before folding over to and re-dissociating on the cross-slip plane; the resulting cross-slipped segment acts as a nucleus, facilitating other segments to switch to the cross-slip plane as well. According to the FL mechanism, with the help of a stair-rod dislocation $1/6\,\langle 110\rangle$ [1], the leading and trailing partial dislocations can simultaneously exist on the secondary and primary planes, respectively; in other words, the stacking faults need not fully constrict at the plane intersection [8]. In face-centered cubic (FCC) systems, atomistic simulations reveal that the detailed process of dislocation cross-slip is determined by a complex local stress state [9].

The dominating mechanism in a given cross-slip process depends on many factors. According to atomic scale simulations of cross-slip in FCC crystals, the FL mechanism is favored in the low temperature, high-stress limit, while the FE mechanism is favored in the high temperature, low-stress limit [10]. For example, a significant amount of dislocations cross slip via the FL mechanism as they propagate through the grain in a nanocrystal subject to a uniaxial tensile stress of 1.6 GPa [11]. Previous NEB calculations in Al show that there exists a critical dislocation line length below which a dislocation segment cross-slips via the FL mechanism, whereas a segment with length above this follows the FE model [7]. In Cu and Ni, which have a lower energy barrier to cross-slip, most atomistic simulations predict the FE mechanism [12, 13]. Nevertheless, based on atomistic simulatoins at 0 K, Duesbery [14] found that cross-slip in Cu via the FL model is possible, provided that the

driving force is large enough. The coupled influences of applied shear stress and dislocation line length on the cross-slip process, especially in the competition between the FL and FE mechanisms, have not been quantified, to the best of our knowledge.

In this paper, we employ both concurrent atomistic-continuum (CAC) [15, 16] and molecular dynamics (MD) methods to simulate the cross-slip process of a single screw dislocation using periodic boundary conditions (PBCs) in FCC Ni. A CAC model, in general, contains a fully resolved atomistic domain and a coarse-grained atomistic domain, in both of which the nucleation and propagation of dislocations and intrinsic stacking faults are addressed using a unified atomistic-continuum integral formulation that relies on the underlying interatomic potential as the only constitutive relation [17]. For dynamic CAC, atomic positions and velocities in the fully atomistic domain are updated following the same rules as in MD; in the coarse-grained domain, a finite element implementation with first order Gaussian quadrature is used to calculate the force on the integration points, whose positions, for a second nearest neighbor (2NN) element, are given in Ref. [16]; then the force at the integration points is used to calculate the force on the nodes, which is then employed to obtain the position and velocity of the nodes at the next time step [15, 18]. Finally, the positions of atoms within each element are linearly interpolated at the end of each step from the nodal positions, which are in turn adopted to update the force on the integration points [16].

The non-singular dislocation core structure/energy and Burgers vector are naturally accommodated in CAC to yield an accurate generalized stacking fault energy (GSFE) surface [16], stress profile, and Peierls stress [19],

without special treatment to remove the singularities of stress and energy at core center, which is needed in dislocation dynamics (DD) [20, 21]. The success of previous calculations in FCC pure metals [22, 23, 24, 19] suggests that CAC is able to simulate dislocation glide. On the other hand, the cross-slip process by which a screw dislocation moves from one slip plane to another has been observed in CAC simulations [25], yet not analyzed quantitatively.

Emphasis in this paper will be placed on (i) how the resolved applied shear stress affects the cross-slip mechanism, and (ii) whether the same dislocation line length-dependence of cross-slip observed for Al applies to Ni. The critical shear stress for cross-slip, which plays an important role in plasticity in crystalline metals, will also be calculated as a function of the dislocation line length. From the methodological viewpoint, we will show the viability of using CAC simulations to accurately model 3-D screw dislocation cross-slip, as a complement to fully resolved atomistic modeling [26], DD [27], crystal plasticity finite element method [28], *ab initio* simulations [29], Peierls-Nabarro type of model [30, 31], and line tension theory [32, 33].

2. Methods

Figure 1 presents the simulation cell for a single screw dislocation cross-slip in a FCC Ni single crystal. The lattice orientations are $x[1\bar{1}\bar{2}]$, $y[110]$, and $z[1\bar{1}1]$. With the lattice parameter $a_0 = 3.52$ Å, the simulation cell has a size of 67.18 nm by 77.66 nm by 68.51 nm. We remark that the same cell is employed in all simulations, except that there are finite elements in the CAC model, as will be described in Section 2.1. In both CAC and MD simulations, the embedded-atom method (EAM) potential of Mishin et al.

[34] is employed for the interatomic force/energy in Ni because the evaluated GSFE is close to the experimentally measured value.

2.1. CAC model

3D rhombohedral elements are used in the coarse-grained domain in the CAC model [15], with surfaces corresponding to {111} slip planes and the jagged interstices of elements at the periodic boundaries filled in with atoms [16], as shown in Fig. 2. Neither displacement continuity nor interelement compatibility is required with this integral formulation [16]. In the coarse-grained domain, all partial dislocations shown in Fig. 2(a–b), on either the primary or the cross-slip plane, contain no pre-existing kink because the [110] dislocation line direction is aligned with the element edge. There is no jog along any dislocation either. This suggests that the CAC model agrees with the classicial cross-slip process without influences of kinks and jogs [13].

In the coarse-grained domain, a uniform element size with cases varying from 125 to 4913 atoms per element is adopted. On the one hand, a larger element size, N_{ape}, results in a smaller number of elements, N_{ele}. On the other hand, a model with a larger element size requires a larger number of atoms to fill in at the periodic boundaries. The net effect is that there exists an element size corresponding to which the number of degrees of freedom (DOF) $N_{\text{DOF}} = 8N_{\text{ele}} + N_{\text{atom}}$ is minimum, where 8 comes from the fact that each element has 8 nodes. As shown in Table 1, the smallest $N_{\text{DOF}}/N_{\text{atom}}^{\text{full}} = 4.87\%$ with $N_{\text{ape}} = 1331$. In Fig. 1, the length of the dislocation line in one periodic cell $L_{\text{d}} = L_y = 77.66$ nm, where L_y is the length of the simulation cell along the y direction. To explore the effect of L_{d}, cases with L_y of 6.47 nm, 12.94 nm, 25.88 nm, 38.83 nm, 51.76 nm, and 64.71 nm, respectively, are also

investigated, while the length of the simulation cell along both the x and z axes remain unchanged.

Table 1: The number of elements N_{ele}, number of atoms N_{atom}, number of degrees of freedom N_{DOF}, and the ratio of N_{DOF} to the number of atoms in a fully resolved atomistic simulation $N_{\text{atom}}^{\text{full}} = 32,902,272$, with varying number of atoms per element N_{ape}. It is found that the value of $N_{\text{DOF}}/N_{\text{atom}}^{\text{full}}$ is not a monotonic function of N_{ele}.

N_{ape}	125	343	729	1331	2197	3375	4913
N_{ele}	258,483	93,280	43,369	23,658	14,218	9,183	6270
N_{atom}	591,897	907,232	1,286,271	1,413,474	1,665,326	1,909,647	2,097,762
N_{DOF}	2,659,761	1,653,472	1,633,223	1,602,738	1,779,070	1,983,111	2,147,922
$N_{\text{DOF}}/N_{\text{atom}}^{\text{full}}$	8.08%	5.03%	4.96%	4.87%	5.41%	6.03%	6.53%

2.2. Atomistic model

An equivalent full atomistic model is constructed by incorporating the same atoms in the atomistic domain of the CAC model and interpolating positions of individual atoms from the nodal positions of each element in the coarse-grained domain in the CAC model, i.e.,

$$\mathbf{R}^k = \boldsymbol{\phi}_{k\xi}\mathbf{x}^{\xi} \tag{1}$$

where $\boldsymbol{\phi}_{k\xi}$ is the trilinear interpolation function, $\mathbf{x}^{\xi}$ and $\mathbf{R}^k$ are the positions of node ξ and atom k, respectively, as shown in Fig. 2(c). There are $N_{\text{atom}}^{\text{full}} = 32,902,272$ atoms in the equivalent full atomistic model, which would be highly computationally intensive.

2.3. Dynamic simulations using both CAC and atomistic models

The problem common to most fs-scale time step dynamic methods, such as MD or dynamic CAC, is the difficulty to capture rare events such as thermally activated cross-slip [35]. Thus, simulations must be carefully designed to capture cross-slip in reasonable wall time. Here, we follow Kang et al. [9] and introduce a straight screw dislocation with Burgers vector $\mathbf{b} = (a_0/2)[110]$ on the primary plane $(\bar{1}11)$; PBCs are applied along both the x and y directions to simulate an array of evenly spaced, infinitely long, initially straight dislocation lines. The boundaries normal to the z axis are assumed traction free, which doesn't strongly affect the line tension of a screw dislocation [36]. After energy minimization, a homogeneous simple shear strain ϵ_{zy} is applied, mainly on the cross-slip plane $(1\bar{1}1)$ and with a small projection on the primary plane, following the idea of Schoeck and Seeger [37]. Note the shear strain is applied within one time step, to avoid the sensitivity of the cross-slip mechanism to strain rate [11]. Then the shear stress is maintained constant under an NPT ensemble at 10 K using a Parrinello-Rahman barostat [38] with time step of 2 fs [25]. Independent simulations with an increment of shear stress $\Delta\tau_{zy} = 10$ MPa are conducted such that the critical shear stress τ_{c} is the minimum stress subject to which the cross-slip event is observed within 50 ps. In some cases with a certain combination of τ_{zy} and L_{d}, a full atomistic simulation, i.e., MD simulation, is performed with the same time step and temperature. We find that the critical stresses determined by low temperature dynamic simulations are close to those calculated by quasistatic simulations, via either quasistatic CAC or molecular statics (MS), yet the dynamic simulations reveal the detailed

cross-slip process.

We emphasize that although the length scale of material volume explored in this work is accessible by classical MD, this is highly computationally expensive to pursue. We will show that CAC simulations can accurately describe the cross-slip process, with a significantly reduced computational cost. To identify dislocations in the coarse-grained domain in the CAC model, the atomic positions are interpolated from the nodal positions before they are processed by the adaptive common neighbor analysis (a-CNA) [39] using OVITO [40]. Some runs are completed using Comet and Bridges on the NSF Extreme Science and Engineering Discovery Environment (XSEDE) [41].

3. Results and discussion

Throughout the remainder of this paper, the superscripts 'pr' and 'cs' are used to distinguish the primary and cross-slip planes, whereas the subscripts 'lead', 'trail', and 'sr' refer to the leading partial, trailing partial, and stair-rod dislocations, respectively.

3.1. Dislocation dissociation

In both atomistic and coarse-grained domains, a full screw dislocation on the primary plane is dissociated into two 30° Shockley partial dislocations, i.e.,

$$\frac{1}{2}a_0[110]^{\mathrm{pr}} \rightarrow \frac{1}{6}a_0[12\bar{1}]^{\mathrm{pr}}_{\mathrm{lead}} + \frac{1}{6}a_0[211]^{\mathrm{pr}}_{\mathrm{trail}} \tag{2}$$

which is energetically favorable according to Frank's rule [20]. The force per unit length on a partial dislocation can be obtained by the Peach-Koehler (PK) formula: $\mathbf{F} = (\mathbf{b} \cdot \boldsymbol{\sigma}) \times \mathbf{t}$, where $\boldsymbol{\sigma}$ is the applied shear stress tensor

whose only non-zero components are τ_{yz} and τ_{zy}, $\mathbf{t} = (1/\sqrt{2})[110]$ is the unit tangent vector of the dislocation line. It is found that as the two partials have Burgers vector with the same screw but opposite edge components, the applied stress acts on the screw components to translate the stacking fault ribbon rigidly, while on the edge components to compress the ribbon [4].

On the cross-slip plane, the same full dislocation splits into a different set of two 30° Shockley partials, i.e.,

$$\frac{1}{2}a_0[110]^{\text{cs}} \rightarrow \frac{1}{6}a_0[21\bar{1}]^{\text{cs}}_{\text{lead}} + \frac{1}{6}a_0[121]^{\text{cs}}_{\text{trail}} \tag{3}$$

where the stacking fault ribbon is expanded by the Escaig stress [5] on the edge components of the partials according to the PK formula.

A dislocation extraction algorithm (DXA) [42] is employed to distinguish the FE mechanism, in which the dislocation is fully constricted at the plane intersection, from the FL mechanism, in which a stair-rod dislocation is formed at the intersection. The DXA is based on a discrete Burgers circuit integral over the elastic displacement field and is able to distinguish a fully constricted dislocation with Burgers vector $(a_0/2)\langle 110\rangle$ from a stair-rod dislocation with Burgers vector $(a_0/6)\langle 110\rangle$.

3.2. Cross-slip via the Fleischer (FL) mechanism

As stated before, the FE mechanism requires the two Shockley partials to be fully constricted at the plane intersection, before the full dislocation is re-dissociated onto the cross-slip plane. Conceptually, such a process can be well accommodated in CAC because both partial and full dislocations are on $\{111\}$ planes. Indeed, a screw dislocation segment changing its slip plane via the FE mechanism have been presented in our previous CAC work [23,

25]. The FL mechanism, however, involves a stair-rod dislocation $(a_0/6)[\bar{1}10]$ on (001) plane, which doesn't belong to the set of $\{111\}$ planes exhibited between elements (Fig. 2). Thus, a question arises as to whether the FL mechanism can be simulated in the coarse-grained domain in CAC.

In a perfect lattice without a dislocation, as illustrated by a 2-D model in Fig. 3(a), four nodes (labeled A, B, C, and D), each of which belongs to a different element, are located adjacent to each other. Then at the plane intersection, denoted by the black cross in Fig. 3(a), the leading partial on the primary plane $\mathbf{b}^{\text{pr}}_{\text{lead}}$ splits into a stair-rod dislocation $\mathbf{b}_{\text{sr}}$ and the leading partial on the cross-slip plane $\mathbf{b}^{\text{cs}}_{\text{lead}}$, i.e.,

$$\frac{1}{6}a_0[12\bar{1}]^{\text{pr}}_{\text{lead}} \rightarrow \frac{1}{6}a_0[\bar{1}10]_{\text{sr}} + \frac{1}{6}a_0[21\bar{1}]^{\text{cs}}_{\text{lead}} \tag{4}$$

which is illustrated in Fig. 3(b), where the overall Burgers vector $\mathbf{b}^{\text{pr}}_{\text{lead}}$ is exhibited by displacing the node B while fixing the other three nodes. It follows that the trailing partial on the primary plane $\mathbf{b}^{\text{pr}}_{\text{trail}}$ reacts with $\mathbf{b}_{\text{sr}}$ to form the trailing partial on the cross-slip plane $\mathbf{b}^{\text{cs}}_{\text{trail}}$, i.e.,

$$\frac{1}{6}a_0[\bar{1}10]_{\text{sr}} + \frac{1}{6}a_0[211]^{\text{pr}}_{\text{trail}} \rightarrow \frac{1}{6}a_0[121]^{\text{cs}}_{\text{trail}} \tag{5}$$

which is illustrated in Fig. 3(c) and the resulting Burgers vector is $\mathbf{b}^{\text{cs}}_{\text{trail}}$. In the end, the trailing partial glides on the cross-slip plane, away from the plane intersections, leaving behind the perfect lattice in Fig. 3(d). In Fig. 3(b–d), node B is displaced by the black arrow in each subfigure while the other three nodes are fixed; after Fig. 3(d), node B is restored to its original position shown in Fig. 3(a) — in other words, the vector sum of the three black arrows in Fig. 3(b–d) is zero.

In the procedure described above, worth further discussion is the movement of node B along the $[\bar{1}10]$ direction on the (001) plane: the corresponding displacement is left after the leading partial dislocation on the cross-slip plane $\mathbf{b}_{\text{lead}}^{\text{cs}}$ glides away, i.e., after Eq. 4, but before the trailing partial dislocation on the primary plane $\mathbf{b}_{\text{trail}}^{\text{pr}}$ reacts with the stair-rod dislocation $\mathbf{b}_{\text{sr}}$, i.e., before Eq. 5. At first glance, node B moving on a (001) plane is contradictory to the assumption that only {111} planes exist between elements in the coarse-grained domain. Nevertheless, such a process is possible because node B (i) can move along any direction with respect to the other three nodes and (ii) only moves by a very short distance $(a_0/6)[\bar{1}10]$ such that it doesn't overlap with the neighboring elements; moreover, each element in the coarse-grained domain in CAC is a nonlocal hyperelastic body and overlap between elements is impossible [16]. In other words, the stair-rod dislocation is formed by both sliding and separation of the node B with respect to the other three nodes, as shown in Fig. 3(e). Although the structural reconstruction is more limited in the coarse-grained domain than in the atomistic domain, moving node B by a short distance doesn't require a much higher stress, as will be discussed in Section 3.3.

3.3. Applied shear stress-dependent cross-slip

The applied shear stress τ_{zy} has a small projection on the primary plane, $\tau_{zy}^{\text{pr}} = \tau_{zy}\cos\theta$, to overcome the Peierls stress σ_{P} and drive dislocation glide, where $\theta = 70.53°$ is the acute angle formed between the primary and cross-slip planes. Thus, $\tau_{zy}^{\text{pr}} = (1/3)\tau_{zy}$.

The critical shear stress for the cross-slip via the FE and FL mechanisms are denoted as $\tau_{\text{c}}^{\text{FE}}$ and $\tau_{\text{c}}^{\text{FL}}$, respectively. In the case of $L_{\text{d}} = 77.66$ nm, the

following events are observed as τ_{zy} increases:

1. $\tau_{zy}^{\mathrm{pr}} < \sigma_{\mathrm{P}}$: the dislocation on the primary plane doesn't move;
2. $\tau_{zy}^{\mathrm{pr}} \geq \sigma_{\mathrm{P}}$ and $\tau_{zy} < \tau_{\mathrm{c}}^{\mathrm{FE}}$: the dislocation on the primary plane moves toward the negative z direction without cross-slip;
3. $\tau_{\mathrm{c}}^{\mathrm{FE}} \leq \tau_{zy} < \tau_{\mathrm{c}}^{\mathrm{FL}}$: the dislocation on the primary plane cross-slips via the FE mechanism;
4. $\tau_{zy} \geq \tau_{\mathrm{c}}^{\mathrm{FL}}$: the dislocation on the primary plane cross-slips via the FL mechanism.

The snapshots of dislocation cross-slip via the FE and FL mechanisms are shown in Fig. 4 and Fig. 5, respectively, for both MD and CAC simulations with $N_{\mathrm{ape}} = 1331$, in the case of $L_{\mathrm{d}} = 77.66$ nm. For the FE mechanism, segments near the center of the dislocation line, indicated by arrows in Fig. 4(a) and (d), bow out first. As a result, curved dislocations glide on the cross-slip plane. Note that it is not the bowing of the dislocation, but the expansion of the stacking fault ribbon on the cross-slip plane or reduction in enthalpy, that supplies the driving force [5, 43]. For the FL mechanism (Fig. 5), the whole dislocation line folds over the plane intersection altogether, with the help of a stair-rod dislocation. In both MD and CAC, the critical shear stress for the FE mechanism is always smaller than that for the FL mechanism, i.e., $\tau_{\mathrm{c}}^{\mathrm{FE}} < \tau_{\mathrm{c}}^{\mathrm{FL}}$, because the creation of a stair-rod dislocation in the FL process is more energetically expensive than the recombination of two partials in the FE process [44]. Moreover, the FE mechanism has a limited stress regime($\sim$ 40 MPa), above which the cross-slip follows the FL process. This suggests that (i) the interpretation of atomistic simulations of cross-slip in terms of mechanism should be made carefully and (ii) near-threshold shear

stress needs to be applied to promote the FE process.

For both mechanisms, the CAC simulations accurately give the key characteristic of the cross-slip, yet the critical shear stresses are higher than MD results, as shown in Fig. 6. Dislocations are less relaxed in the coarse-grained domain such that (i) a higher stress is required to form the stair-rod dislocation and (ii) compressing or expanding the stacking fault requires a higher Escaig stress [16]. However, we note that the trends are monotonic and convergent with regard to coarse-graining error. The finding that cross-slip is easier to operate based on MD simulations agrees with the fact that the cross-slip is favored when the applied stress increases the width of the stacking fault ribbon in the cross-slip plane while decreasing it on the primary plane [4]. Nevertheless, we emphasize that (i) the relative error in τ_c between MD and CAC with $\sqrt[3]{N_{\text{ape}}} = 11$, i.e., $N_{\text{ape}} = 1331$ which has the fewest DOF according to Table 1, is about 8.09% and 7.86% for the FE and FL mechanisms, respectively, and (ii) both τ_c converge to the atomistics as the elements become smaller and contain fewer atoms, as shown in Fig. 6.

The level of stress predicted from our CAC and MD simulations for cross-slip is at GPa level. Although this is comparable to that from MD simulations in the literature [9, 45], it is significantly higher than that in experiments in FCC pure metals. There are two major reasons that may contribute to the overestimation of the critical stress:

1. In this work, the shear strain is applied to the CAC and MD models and the process is stress-driven and largely athermal. Cross-slip typically occurs in these simulations within a few picoseconds, and is not thermally activated. The reaction pathway for the thermally activated

cross-slip process is well-preserved, on the other hand. As a consequence, the critical stress predicted from CAC or MD is much higher than the measurement in traditional low-strain-rate experiments at much longer times during which thermal fluctuations have high enough probability to drive cross-slip. This does not mean that the simulations in this paper are in any way inaccurate or aphysical — they simply reflect the limiting case of essentially athermal, stress-driven cross-slip along the same reaction pathway. In the current CAC approach, the time step size is established based on the requirements of the fully atomistic domain to ensure accuracy. To reduce the strain rate in these dynamic simulations, a multi-time-scaling algorithm is required to increase the time step in coarse-grain domains and is the subject of ongoing work.

2. In experiments, dislocation density is relatively high and cross-slip occurs with the influence of dislocation interactions and internal stresses in contrast to the case of cross-slip of an isolated screw dislocation considered in our simulations. As such, the critical cross-slip stress predicted in this paper is expected to provide an upper bound.

3.4. Dislocation line length-dependent cross-slip

We then study the cross-slip process for different dislocation line lengths, L_{d}, as shown in Fig. 7. When $L_{\mathrm{d}} > 20$ nm, dynamic CAC simulations with $N_{\mathrm{ape}} = 1331$ are carried out; otherwise MD simulations are performed. Because of the difference in τ_{zy} between MD and CAC, an analysis of the variation of τ_{zy} as a function of L_{d} is more meaningful within each type of simulation. It is found that as L_{d} increases, both $\tau_{\mathrm{c}}^{\mathrm{FE}}$ and $\tau_{\mathrm{c}}^{\mathrm{FL}}$ decrease. This

suggests that, like in Al [7], the energy barrier for cross-slip in Ni is dislocation line length-dependent. Moreover, MD simulations show that while both FE and FL types of cross-slip operate at different τ_{zy} in the case of $L_{\mathrm{d}} = 12.94$ nm, the dislocation only cross-slips via the FL mechanism for $L_{\mathrm{d}} = 6.47$ nm. In comparison, we note that (i) Kang et al. [9] observed dislocation cross-slip via the FE mechanism for $L_{\mathrm{d}} = 10.56$ nm in Ni using NEB and (ii) the critical dislocation line length between the FE and FL mechanisms is 6.3 nm in Al [7].

4. Conclusions

In this paper, dynamic CAC and MD simulations are performed to study the shear stress- and line length-dependent screw dislocation cross-slip in FCC Ni. Results are summarized as follows:

1. At a significantly reduced computational cost, CAC simulations can accurately describe the pathway of the cross-slip process via both FE and FL mechanisms as obtained via MD, as well as predict reasonably accurate critical shear stresses for cross-slip operation.
2. In the case of a dislocation of length 77.66 nm subject to a constant applied shear stress of increasing values, the following events operate consecutively: (i) the dislocation begins to move once the resolved shear stress on the primary plane overcomes the Peierls stress, (ii) the dislocation cross-slips via the FE mechanism, and (iii) the dislocation cross-slips via the FL mechanism. This suggests that the cross-slip process is applied shear stress-dependent.

3. The dislocation cross-slip mechanism, manifested by the relevant critical shear stress, is also line length-dependent. In particular, the FE mechanism is not observed for a short dislocation line of 6.47 nm, but for a longer dislocation of 12.94 nm. Moreover, a longer dislocation line has a slightly lower critical shear stresses for cross-slip operation.

We remark that both the low temperature dynamic and quasistatic simulations can only calculate the critical stress for an event, e.g., dislocation gliding, cross-slip, but not its energy barrier [46]. The nudged elastic band (NEB) method [47], which has been employed to quantify the activation energy of cross-slip [9, 7, 13, 48, 49], can be applied with CAC to explore the energy barrier and more detailed minimum energy pathway for much more extended dislocations at the submicron and micron scales. We also note that only the bulk dislocation cross-slip via an acute angle is investigated in this paper. Other types of cross-slip, such as surface and intersection cross-slip [27], via an obtuse angle, which has a higher activation energy and, for the FL mechanism, a stair-rod dislocation of (1/6)[200] type [6], will receive our future attention. The issue of screw dislocations cross-slip in a single pile-up, which involves a length scale inaccessible to classical atomistic simulations, will be explored using CAC as well — such a simulation is expected to provide an important input to the higher scale theory or simulation tool.

Acknowledgments

These results are based upon work supported by the National Science Foundation as a collaborative effort between Georgia Tech (CMMI-1232878) and University of Florida (CMMI-1233113). Any opinions, findings, and

conclusions or recommendations expressed in this material are those of the authors and do not necessarily reflect the views of the National Science Foundation. LX acknowledges the support from the Department of Energy, Office of Basic Energy Sciences under Award Number DE-SC0006539. The work of LX was also supported in part by the National Science Foundation under Award Number CMMI-1536925. The authors thank Dr. Dengke Chen and Mr. Luke Costello for helpful discussions, and thank Dr. Alexander Stukowski for providing the dislocation extraction algorithm code. This work used the Extreme Science and Engineering Discovery Environment (XSEDE), which is supported by National Science Foundation grant number ACI-1053575.

References

[1] D. Hull, D. J. Bacon, Introduction to Dislocations, 5th ed., Butterworth-Heinemann, 2011.

[2] C. V. Singh, A. J. Mateos, D. H. Warner, Atomistic simulations of dislocationprecipitate interactions emphasize importance of cross-slip, Scripta Mater. 64 (2011) 398–401.

[3] T. Hatano, T. Kaneko, Y. Abe, H. Matsui, Void-induced cross slip of screw dislocations in fcc copper, Phys. Rev. B 77 (2008) 064108.

[4] B. R. Ramírez, N. Ghoniem, G. Po, Ab initio continuum model for the influence of local stress on cross-slip of screw dislocations in fcc metals, Phys. Rev. B 86 (2012) 094115.

[5] B. Escaig, Sur le glissement dvi des dislocations dans la structure cubique faces centres, J. Phys. 29 (1968) 225–239.

[6] R. L. Fleischer, Cross slip of extended dislocations, Acta Metall. 7 (1959) 134–135.

[7] C. Jin, Y. Xiang, G. Lu, Dislocation cross-slip mechanisms in aluminum, Philos. Mag. 91 (2011) 4109–4125.

[8] M. J. Buehler, A. Hartmaier, H. Gao, M. A. Duchaineau, F. F. Abraham, The dynamical complexity of work-hardening: a large-scale molecular dynamics simulation, Acta Mech. Sinica 21 (2005) 103–111.

[9] K. Kang, J. Yin, W. Cai, Stress dependence of cross slip energy barrier for face-centered cubic nickel, J. Mech. Phys. Solids 62 (2014) 181–193.

[10] W. Cai, V. V. Bulatov, J. Chang, J. Li, S. Yip, Dislocation core effects on mobility, in: J. Hirth, F. Nabarro (Eds.), Dislocations in Solids, volume 12, Elsevier, 2005, pp. 1–80. URL: http://www.sciencedirect.com/science/article/pii/S1572485905800038.

[11] E. Bitzek, C. Brandl, P. M. Derlet, H. Van Swygenhoven, Dislocation cross-slip in nanocrystalline fcc metals, Phys. Rev. Lett. 100 (2008) 235501.

[12] T. Rasmussen, K. W. Jacobsen, T. Leffers, O. B. Pedersen, Simulations of the atomic structure, energetics, and cross slip of screw dislocations in copper, Phys. Rev. B 56 (1997) 2977–2990.

[13] S. I. Rao, D. M. Dimiduk, J. A. El-Awady, T. A. Parthasarathy, M. D. Uchic, C. Woodward, Screw dislocation cross slip at cross-slip plane jogs and screw dipole annihilation in FCC Cu and Ni investigated via atomistic simulations, Acta Mater. 101 (2015) 10–15.

[14] M. S. Duesbery, Dislocation motion, constriction and cross-slip in fcc metals, Modelling Simul. Mater. Sci. Eng. 6 (1998) 35.

[15] L. Xiong, G. Tucker, D. L. McDowell, Y. Chen, Coarse-grained atomistic simulation of dislocations, J. Mech. Phys. Solids 59 (2011) 160–177.

[16] S. Xu, R. Che, L. Xiong, Y. Chen, D. L. McDowell, A quasistatic implementation of the concurrent atomistic-continuum method for FCC crystals, Int. J. Plast. 72 (2015) 91–126.

[17] Y. Chen, Reformulation of microscopic balance equations for multiscale materials modeling, J. Chem. Phys. 130 (2009) 134706.

[18] L. Xiong, J. Rigelesaiyin, X. Chen, S. Xu, D. L. McDowell, Y. Chen, Coarse-grained elastodynamics of fast moving dislocations, Acta Mater. 104 (2016) 143–155.

[19] S. Xu, L. Xiong, Y. Chen, D. L. McDowell, An analysis of key characteristics of the Frank-Read source process in FCC metals, J. Mech. Phys. Solids 96 (2016) 460–476.

[20] J. P. Hirth, J. Lothe, Theory of Dislocations, Krieger Pub Co, 1992.

[21] W. Cai, A. Arsenlis, C. R. Weinberger, V. V. Bulatov, A non-singular continuum theory of dislocations, J. Mech. Phys. Solids 54 (2006) 561–587.

[22] L. Xiong, S. Xu, D. L. McDowell, Y. Chen, Concurrent atomistic-continuum simulations of dislocation-void interactions in fcc crystals, Int. J. Plast. 65 (2015) 33–42.

[23] S. Xu, L. Xiong, Y. Chen, D. L. McDowell, Sequential slip transfer of mixed-character dislocations across Σ3 coherent twin boundary in FCC metals: a concurrent atomistic-continuum study, npj Comput. Mater. 2 (2016) 15016.

[24] S. Xu, L. Xiong, Y. Chen, D. L. McDowell, Edge dislocations bowing out from a row of collinear obstacles in Al, Scripta Mater. 123 (2016) 135–139.

[25] S. Xu, L. Xiong, Q. Deng, D. L. McDowell, Mesh refinement schemes for the concurrent atomistic-continuum method, Int. J. Solids Struct. 90 (2016) 144–152.

[26] M. Li, W. Y. Chu, K. W. Gao, L. J. Qiao, Molecular dynamics simulation of cross-slip and the intersection of dislocations in copper, J. Phys.: Condens. Matter 15 (2003) 3391.

[27] A. M. Hussein, S. I. Rao, M. D. Uchic, D. M. Dimiduk, J. A. El-Awady, Microstructurally based cross-slip mechanisms and their effects on dislocation microstructure evolution in fcc crystals, Acta Mater. 85 (2015) 180–190.

[28] A. Alankar, D. P. Field, H. M. Zbib, Explicit incorporation of cross-slip in a dislocation density-based crystal plasticity model, Philos. Mag. 92 (2012) 3084–3100.

[29] C. Woodward, S. I. Rao, Ab-initio simulation of isolated screw dislocations in bcc Mo and Ta, Philos. Mag. A 81 (2001) 1305–1316.

[30] G. Lu, V. V. Bulatov, N. Kioussis, Dislocation constriction and cross-slip: An *ab initio* study, Phys. Rev. B 66 (2002) 144103.

[31] A. H. W. Ngan, On generalizing the Peierls-Nabarro model for screw dislocations with non-planar cores, Philos. Mag. Lett. 72 (1995) 207–213.

[32] Y. Q. Sun, Line tension of screw dislocations on cross-slip planes, Philos. Mag. Lett. 74 (1996) 175–188.

[33] L. Proville, S. Patinet, Atomic-scale models for hardening in fcc solid solutions, Phys. Rev. B 82 (2010) 054115.

[34] Y. Mishin, D. Farkas, M. J. Mehl, D. A. Papaconstantopoulos, Interatomic potentials for monoatomic metals from experimental data and *ab initio* calculations, Phys. Rev. B 59 (1999) 3393–3407.

[35] A. F. Voter, F. Montalenti, T. C. Germann, Extending the time scale in atomistic simulation of materials, Annu. Rev. Mater. Res. 32 (2002) 321–346.

[36] F. Pavia, W. A. Curtin, Parallel algorithm for multiscale atomistic/continuum simulations using LAMMPS, Modelling Simul. Mater. Sci. Eng. 23 (2015) 055002.

[37] T. Rasmussen, Cross slip in the face centred cubic structure: An atomistic approach, in: J. Lpinoux, D. Mazire, V. Pontikis, G. Saada (Eds.), Multiscale Phenomena in Plasticity: From Experiments to Phenomenology, Modelling and Materials Engineering, number 367 in NATO Science Series, Springer Netherlands, 2000, pp. 281–292. URL: http://

link.springer.com/chapter/10.1007/978-94-011-4048-5_22, dOI: 10.1007/978-94-011-4048-5_22.

[38] M. Parrinello, A. Rahman, Polymorphic transitions in single crystals: A new molecular dynamics method, J. Appl. Phys. 52 (1981) 7182–7190.

[39] A. Stukowski, Structure identification methods for atomistic simulations of crystalline materials, Modelling Simul. Mater. Sci. Eng. 20 (2012) 045021.

[40] A. Stukowski, Visualization and analysis of atomistic simulation data with OVITO—the Open Visualization Tool, Modelling Simul. Mater. Sci. Eng. 18 (2010) 015012.

[41] J. Towns, T. Cockerill, M. Dahan, I. Foster, K. Gaither, A. Grimshaw, V. Hazlewood, S. Lathrop, D. Lifka, G. Peterson, R. Roskies, J. Scott, N. Wilkins-Diehr, XSEDE: Accelerating scientific discovery, Comput. Sci. Eng. 16 (2014) 62–74.

[42] A. Stukowski, V. V. Bulatov, A. Arsenlis, Automated identification and indexing of dislocations in crystal interfaces, Modelling Simul. Mater. Sci. Eng. 20 (2012) 085007.

[43] G. Schoeck, The cross-slip energy unresolved, Philos. Mag. Lett. 89 (2009) 505–515.

[44] A. J. E. Foreman, Dislocation energies in anisotropic crystals, Acta Metall. 3 (1955) 322–330.

[45] S. I. Rao, D. M. Dimiduk, J. A. El-Awady, T. A. Parthasarathy, M. D. Uchic, C. Woodward, Activated states for cross-slip at screw dislocation intersections in face-centered cubic nickel and copper via atomistic simulation, Acta Mater. 58 (2010) 5547–5557.

[46] R. Gröger, V. Vitek, Multiscale modeling of plastic deformation of molybdenum and tungsten. III. Effects of temperature and plastic strain rate, Acta Mater. 56 (2008) 5426–5439.

[47] R. Gröger, V. Vitek, Constrained nudged elastic band calculation of the Peierls barrier with atomic relaxations, Modelling Simul. Mater. Sci. Eng. 20 (2012) 035019.

[48] T. Rasmussen, K. W. Jacobsen, T. Leffers, O. B. Pedersen, S. G. Srinivasan, H. Jónsson, Atomistic determination of cross-slip pathway and energetics, Phys. Rev. Lett. 79 (1997) 3676–3679.

[49] T. Vegge, Atomistic simulations of screw dislocation cross slip in copper and nickel, Mater. Sci. Eng. A 309310 (2001) 113–116.

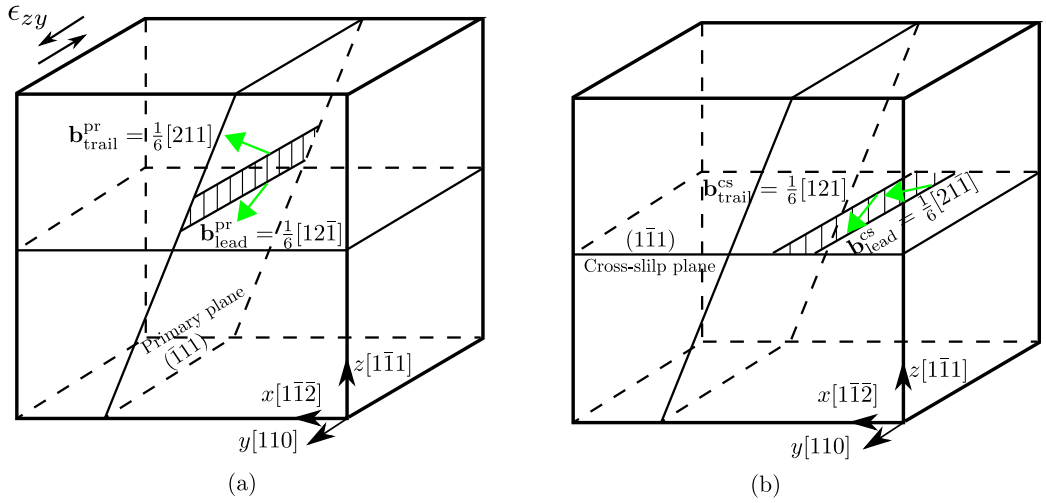

Figure 1: Simulation cell for dislocation cross-slip. (a) A single screw dislocation splits into two 30° Shockley partial dislocations on the primary slip plane $(\bar{1}11)$. (b) Subject to a shear strain ϵ_{zy}, the screw dislocation switches to the cross-slip plane $(1\bar{1}1)$ and is dissociated into another set of two Shockley partials.

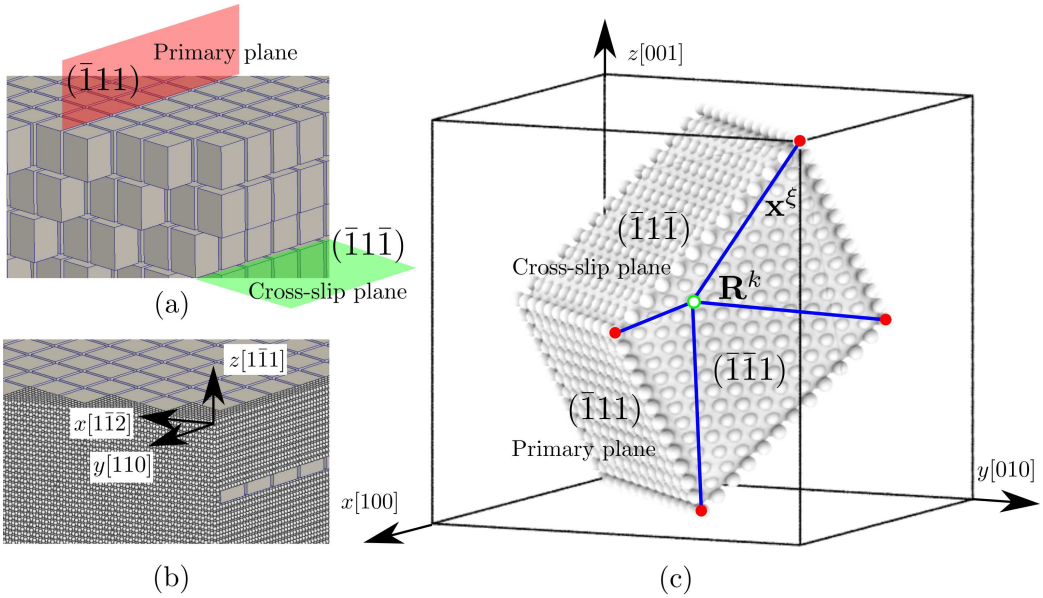

Figure 2: In a CAC model with $N_{\text{ape}} = 729$, (a) only the coarse-grained domain with discontinuous rhombohedral elements is shown and (b) atoms are filled in at the periodic boundaries along both the x and y directions. (c) A 3-D rhombohedral element with faces on {111} planes, the slip planes of FCC lattice. The positions of atoms within each element, e.g., the green open circle, are interpolated from the nodal positions (red solid circles).

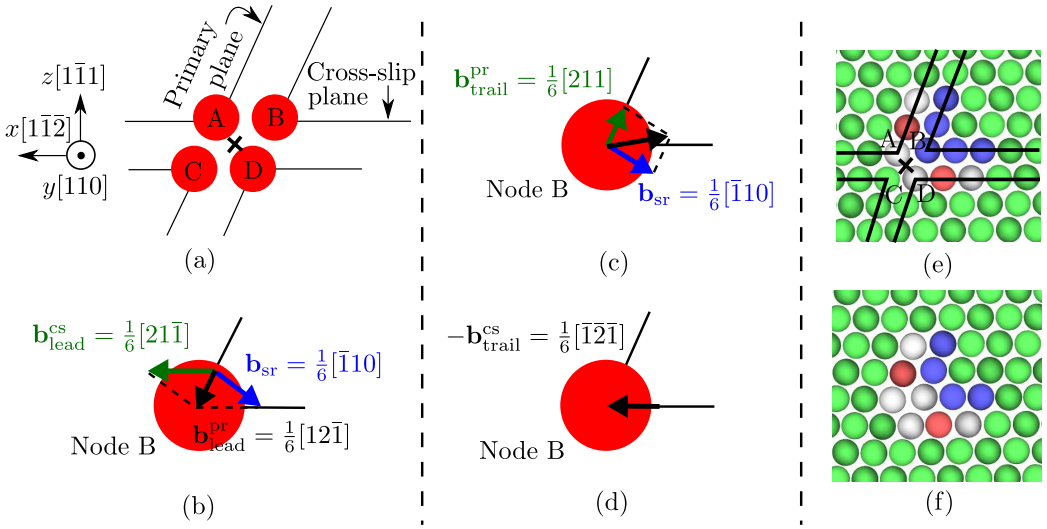

Figure 3: (a) A 2D illustration of four nodes (A, B, C, and D) belonging to adjacent elements in a perfect lattice without a dislocation; the black cross denotes the line of intersection between the primary and cross-slip planes. (b) According to Eq. 4, the leading partial dislocation on the primary slip plane $\mathbf{b}^{\mathrm{pr}}_{\mathrm{lead}}$ (black arrow) splits into the leading partial dislocation on the cross-slip plane $\mathbf{b}^{\mathrm{cs}}_{\mathrm{lead}}$ (green arrow) and a stair-rod dislocation $\mathbf{b}_{\mathrm{sr}}$ (blue arrow). (c) According to Eq. 5, the trailing partial dislocation on the primary plane $\mathbf{b}^{\mathrm{pr}}_{\mathrm{trail}}$ (green arrow) reacts with the stair-rod dislocation $\mathbf{b}_{\mathrm{sr}}$ (blue arrow) to form the trailing partial dislocation on the cross-slip plane $\mathbf{b}^{\mathrm{cs}}_{\mathrm{trail}}$. (d) The trailing partial dislocation $\mathbf{b}^{\mathrm{cs}}_{\mathrm{trail}}$ glides on the cross-slip plane away from the line of intersection, leaving behind the same perfect lattice as in (a). Note that only the edge components of partial dislocations are shown because their screw components are pointing outward along the positive y direction. Atomic configurations of the dislocation folding over the plane intersection via the FL mechanism in (e) the coarse-grained and (f) atomistic domains are also shown. The four nodes (A, B, C, and D) and the cross in (e) correspond to those in (a).

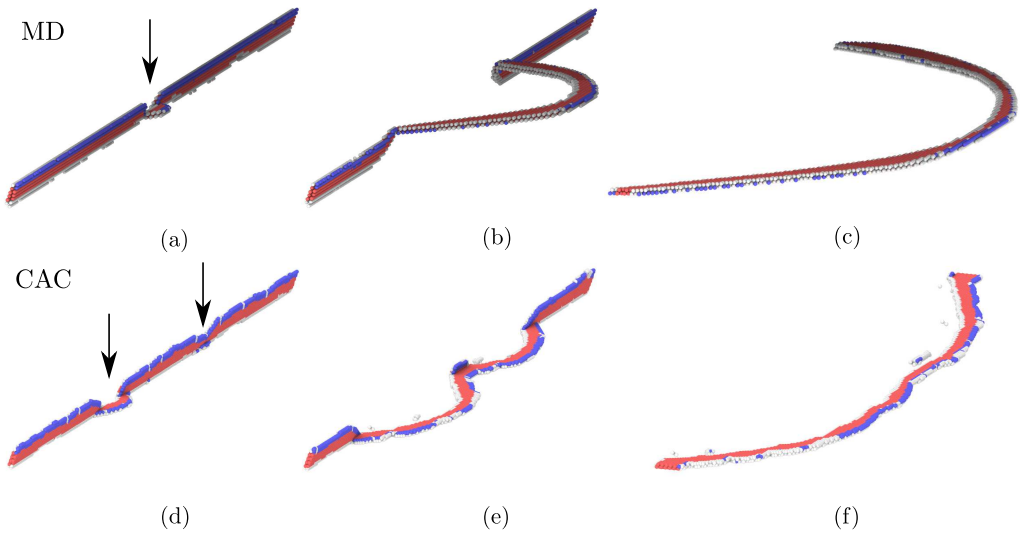

Figure 4: Cross-slip of a screw dislocation via the FE mechanism subject to a shear stress of (a–c) 1.36 GPa in MD and (d–f) 1.47 GPa in CAC with $N_{\text{ape}} = 1331$. The initial length of the dislocation line in one periodic cell $L_{\text{d}} = 77.66$ nm. Segments near the center of the dislocation line, indicated by arrows in (a) and (d), bow out first.

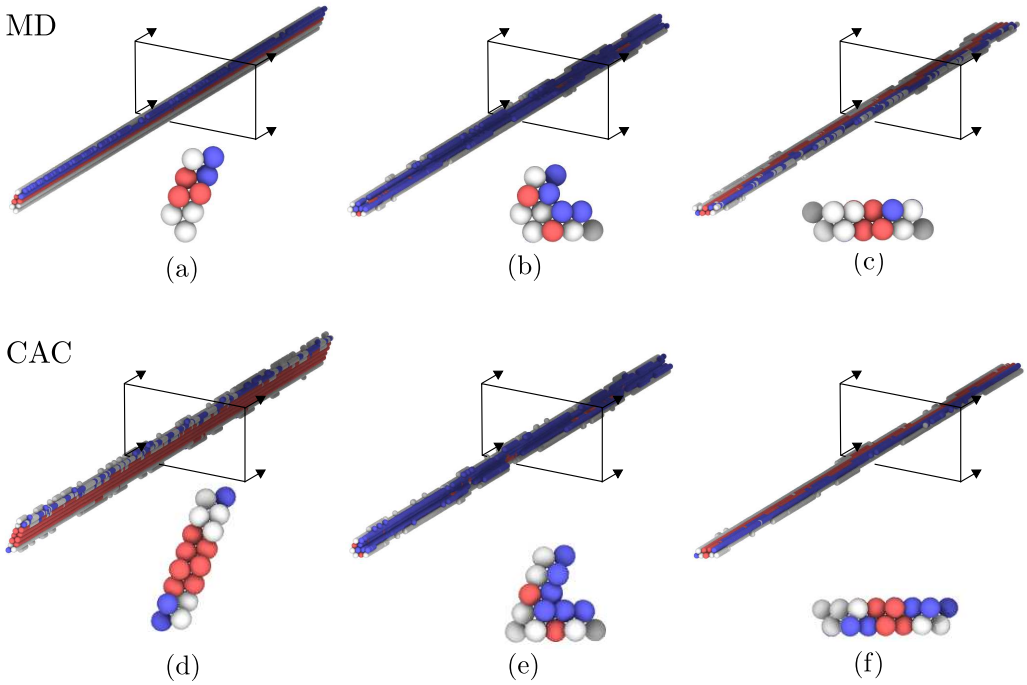

Figure 5: Cross-slip of a screw dislocation via the FL mechanism subject to a shear stress of (a–c) 1.4 GPa in MD and (d–f) 1.51 GPa in CAC with $N_{\text{ape}} = 1331$. The initial length of the dislocation line in one periodic cell $L_{\text{d}} = 77.66$ nm. Cross-sections of the dislocation line at the center are shown, where CAC gives a wider stacking fault than MD.

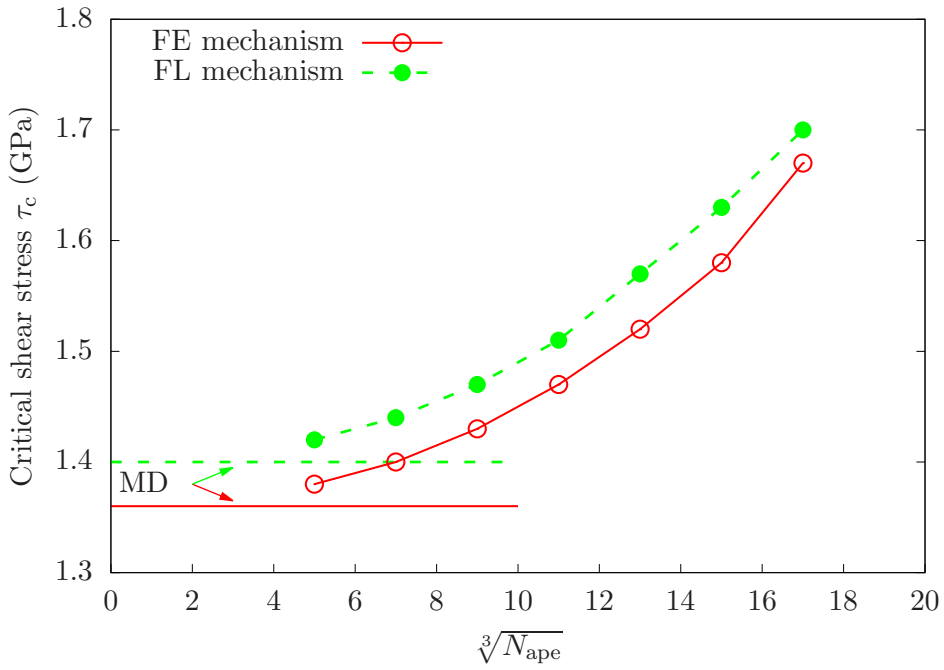

Figure 6: The critical shear stress τ_c for both FE and FL mechanisms as a function of the number of atoms per element N_{ape} in CAC simulations, compared with the results obtained by MD simulations which are indicated by the horizontal lines. It is shown that for both mechanisms, τ_c converges to the atomistics as the elements become smaller and contain fewer atoms. The initial length of the dislocation line in one periodic cell $L_d = 77.66$ nm.

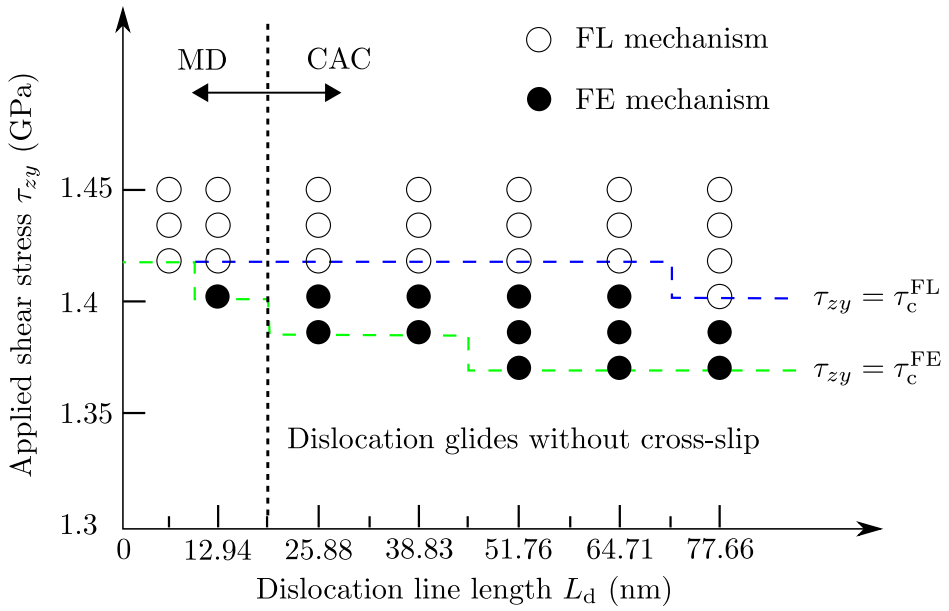

Figure 7: Dislocation behavior as a function of both the applied shear stress τ_{zy} and dislocation line length $L_{\rm d}$. It is found that with an increasing τ_{zy}, dislocatioan begins to move but without cross-slip; at a higher τ_{zy}, it cross-slips via the FE or FL mechanisms. The critical stresses for cross-slip, $\tau_{\rm c}^{\rm FE}$ and $\tau_{\rm c}^{\rm FL}$, are $L_{\rm d}$-dependent. Note that when $L_{\rm d} > 20$ nm, dynamic CAC simulations with $N_{\rm ape} = 1331$ are carried out, otherwise MD simulations are performed instead.